Origin of the Ir–Si Bond Shortening in Ir-NSiN complexes

Pilar García-Orduña,[a] Israel Fernández,[,b] Luis A. Oro[a] and Francisco J. Fernández-Alvarez*[,a]*

Received 00th January 20xx,
Accepted 00th January 20xx

DOI: 10.1039/x0xx00000x

The Ir–Si bond distances reported for Ir-(*fac*-κ³-NSiN^{OPy}) and Ir-(*fac*-κ³-NSiN^{4MeOPy}) species (NSiN^{OPy} = bis(pyridine-2-yloxy)methylsilyl and NSiN^{4MeOPy} = bis(4-methyl-pyridine-2-yloxy)methylsily) are in the range of 2.220-2.235 Å. These values are in the lowest limit of the Ir–Si bond distances found in the Cambridge Structural Database (CSD). To understand the origin of such remarkable shortening, a computational study of the bonding situation of representative examples of Ir-(*fac*-κ³-NSiN) species has been carried out. It is found that the Ir–Si bond can be described as an electron-sharing (i.e. covalent) bond. Despite that, this bond is highly polarized and as a result, the contribution of the electrostatic attractions to the bonding is rather significant. Indeed, there exists a linear relationship (R^2 = 0.97) between the Ir–Si bond distance and the extent of the computed electrostatic interactions, which indicates that the ionic contribution to the bonding is mainly responsible for the observed Ir–Si bond shortening.

Introduction

The chemistry of iridium and rhodium complexes with monoanionic tridentate ESiE-type ligands, where the central silicon atom and the peripheral donor atoms (E = P, N, S) are covalently interconnected by carbon or functionalized-carbon chains, has gained interest in recent years. Their reactivity, catalytic activity and selectivity depend on the nature of the donor groups, the linker chains and the substituents at the silicon atom, and therefore are easily tuneable.[1]

Monoanionic κ³-PSiP ligands coordinate to iridium and rhodium either in *mer*-κ³ or *fac*-κ³-coordination modes (Figure 1).[2-7] Iridium and rhodium complexes with monoanionic κ³-NSiN-type[8,9,10] and κ³-SSiS-type[11] ligands usually show a distorted octahedral geometry with the corresponding ligand in *fac*-κ³-coordination mode (Figure 1).

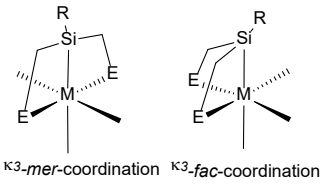

Figure 1. Examples of *mer*-κ³ or *fac*-κ³-coordination of ESiE ligands to transition metal-complexes (E = P, N, S).

The presence of the metal-silyl bond in the above-mentioned complexes labilizes the ligand *trans* located to the silicon atom as a consequence of the known strong *trans*-effect exerted by silyl ligands,[12] which has proven to be a key feature for the reactivity and catalytic activity of such complexes.[1a,3-11]

Rh-(*fac*-κ³-NSiN) and Ir-(*fac*-κ³-NSiN) complexes having bis(pyridine-2-yloxy)methylsilyl (NSiN^{OPy}), bis(4-methyl-pyridine-2-yloxy)methylsilyl (NSiN^{4MeOPy}) and bis(8-quinolyl)methylsilyl (NSiN^{Q}) ligands (Figure 2) stand out for presenting short metal–Si bond lengths.[8,9,10] Indeed, the Ir–Si bond distances found for Ir-(*fac*-κ³-NSiN^{OPy}) and Ir-(*fac*-κ³-NSiN^{4MeOPy}) species, in the range of 2.22-2.24 Å,[8] are among the shortest Ir–Si bond distances so far reported.

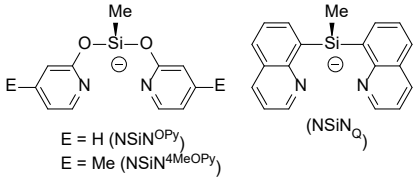

Figure 2. Bis(pyridine-2-yloxy)methylsilyl (NSiN^{OPy}), bis(4-methyl-pyridine-2-yloxy)methylsilyl (NSiN^{4MeOPy}) and bis(8-quinolyl)methylsilyl (NSiN^{Q}) ligands.

The metal-silicon bond lengths in late or low-valent transition-metal silyl complexes are frequently shorter than one would expect for a covalent σ-bond. This fact has usually been attributed to the occurrence of π-backbonding from *d*-metal orbitals to empty silicon orbitals.[13,14] Alternatively, other authors have also invoked the contribution of an ionic component to explain the shortening of metal-silyl bonds.[14,15]

On the other hand, the Ir–Si bond distances found for base-stabilized iridium-silylene and iridium-silyl complexes are commonly in the range of ≈ 2.26–2.32 Å[16-19] and ≈ 2.29–2.41 Å,[20] respectively. Thus, the Ir–Si bond distance is not an accurate criterion to distinguish between iridium-silyl and base-stabilized iridium-silylene bonds. For example, the Ir–Si bonds in iridium complexes with monoanionic κ²-pyridine-2-yloxy-dialkylsilyl ligands (NSi^{R}2, R = Me, ^{i}Pr, ^{t}Bu; Scheme 1), which exhibit Ir–Si bond distances in the 2.25-2.29 Å range,[21,22] have been proposed as intermediate between 2-pyridone-stabilized iridium-silylene and -silyl bonds.[21c] In particular, the Ir–Si bond distances found for Ir-(*fac*-κ³-NSiN^{OPy}) species[8] are below the range of distances so far reported for base-stabilized iridium-silylene species. This might well be a consequence of the presence of two 2-pyridone moieties acting as bridges between the iridium and the two silicon atoms.[21c]

[a] *Departamento de Química Inorgánica-Instituto de Síntesis Química y Catálisis Homogénea (ISQCH), Universidad de Zaragoza–CSIC, Facultad de Ciencias, 50009 Zaragoza, Spain. E-mail, F. J. Fernández-Alvarez: paco@unizar.es*

[b] *Departamento de Química Orgánica I and Centro de Innovación en Química Avanzada, Facultad de Ciencias Químicas, Universidad Complutense de Madrid, 28040-Madrid, Spain. E-mail, I. Fernández: israel@quim.ucm.es*

Electronic Supplementary Information (ESI) available: Figures S1-S3, CCDC search and Cartesian coordiantes. See DOI: 10.1039/x0xx00000x

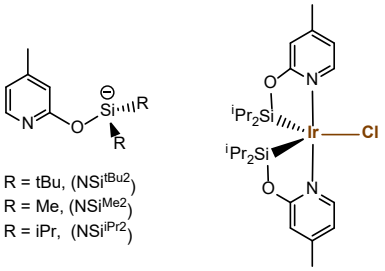

Scheme 1. Monoanionic κ^2-pyridine-2-yloxy-dialkylsilyl ligands (NSi^R, R = Me, ^{i}Pr, ^{t}Bu) and one example of an Ir-NSi^{iPr2} complex.

To shed light on the actual reasons that cause the Ir–Si bond shortening in these complexes, we first present a statistical analysis of the bond distance in iridium complexes having a Ir–Si bond including Ir-(*fac*-κ^3-NSiN) species. Then, the bonding situation of representative Ir-(*fac*-κ^3-NSiN) species has been explored using state-of-the-art computational methods. As described below, our calculations suggest that the electrostatic interactions between the corresponding NSiN ligand and the iridium atom have a direct impact on the corresponding Ir–Si bond length.

Results and Discussion

Ir–Si bond length analysis (CSD Search) and structural comments on Ir-(*fac*-κ^3-NSiN) species

A statistical analysis of the Ir–Si bond lengths included in the Cambridge Structural Database (CSD)[23] using ConQuest 2020.3.0 program[24] has been performed (Table S1). This analysis shows that the mean Ir–Si bond length is 2.34(5) Å, in good agreement with the median value (2.34 Å), indicating a symmetric distribution, with 2 high outliers. Figure 3 shows the statistical distribution of the Ir–Si bond distances (blue in Figure 3) in comparison with those observed in Ir-(*fac*-κ^3-NSiN) species (orange in Figure 3), the latter belonging to the lowest limit.

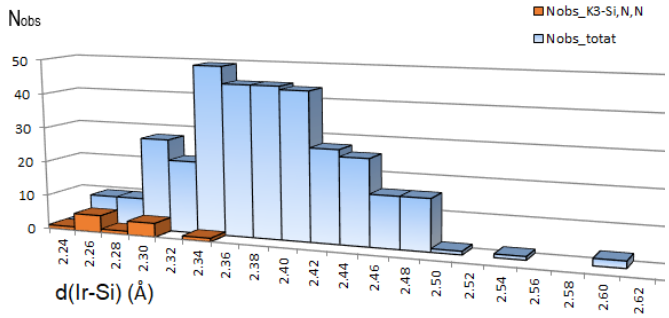

Figure 3. Histogram of Ir–Si bond length reported in the Cambridge Structural Database (CSD). Blue: all the structures. Orange: structures with *fac*-κ^3-*NSiN* coordination.

According to the reported solid-state structures of Ir-(*fac*-κ^3-NSiN) complexes (Figure 4), the iridium atom typically possesses a distorted-octahedral geometry.[8,10] However, an example of a compound exhibiting a distorted-square pyramidal geometry, complex **4** (Figure 4), has also been reported.[10b]

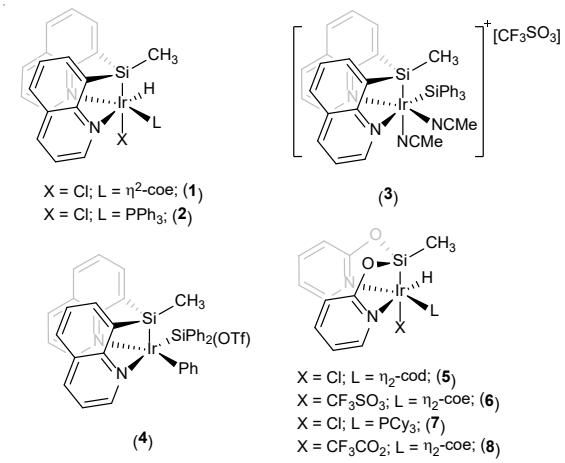

Figure 4. Ir-(*fac*-κ^3-NSiN^Q) and Ir-(*fac*-κ^3-NSiN^{OPy}) mononuclear species whose structure has been published.

Geometrical parameters describing the facial coordination of the tridentate ligand in Ir-(*fac*-κ^3-NSiN) are summarized in Table 1. As a general trend, the deviation of the Si-Ir-N and N-Ir-N bite angles from the ideal 90° value can be observed. This feature is due to the formation of the two five-membered iridacycles, which greatly contribute to the stabilization of the molecular structure. This stabilization seems to be stronger in the Ir-(*fac*-κ^3-NSiN^{OPy}) species, where shorter Ir–Si bond lengths (2.22-2.23 Å) together with acuter N-Ir-N bite angles (N-Ir-N: 79.1-81.9°) are observed,[8] compared to those reported for Ir-(*fac*-κ^3-NSiN^Q) complexes (2.25-2.30 Å and 84.1-83.8°, respectively).[10] This may be illustrated when comparing the geometry of compounds **2** and **7**, both containing a Si atom located *trans* to a chloride ligand.

The data gathered in Table 1 also suggests that the presence of a triflate ligand instead of a chloride ligand in the apical position further contributes to the shortening of the Ir–Si bond. Indeed, the Ir-(*fac*-κ^3-NSiN^{OPy}) complex **6** exhibits the shortest Ir–Si bond length of the entire series (2.22 Å). A similar behaviour is found in the analogous complex **8**, having the apical CF_3CO_2 ligand (2.22 Å). Despite that, very little is known about the actual factors leading to this significant shortening of the Ir–Si bond distances, which prompted us to perform a computational study on the bonding situation of these particular Ir-(*fac*-κ^3-NSiN) species.

Table 1. Ir–Si bond lengths (Å) and selection of angles (°) for Ir-(*fac*-κ³-NSiN) complexes.

Comp./(L)	N-Ir-N (°)	Si-Ir-N (°)	Ir–Si (Å)	ref
1/($NSiN^{Q}$)	87.5(3)	83.2 (2); 83.3(2)	2.275(3)	10a
2/($NSiN^{Q}$)	85.3(2)	84.1(2); 82.3(2)	2.278 (2)	10a
3/($NSiN^{Q}$)	89.7(9)	82.82(7); 83.82(8)	2.3032(9)	10b
4/($NSiN^{Q}$)	86.3(2)	83.0(2); 83.7(2)	2.252(2)	10b
5/($NSiN^{OPy}$)	86.3(1)	80.6(1); 79.9(1)	2.236(1)	8d
6/($NSiN^{OPy}$)	85.7(1)[a]	79.8(1); 81.6(1)[a]	2.219(1)[a]	8a
	86.7(1)[b]	80.7(1); 80.7(1)[b]	2.228(2)[b]	
7/($NSiN^{OPy}$)	85.7(1)	80.2(1); 79.1(1)	2.224(1)	8d
8/($NSiN^{OPy}$)	84.9(3)	80.2(2); 81.2(2)	2.223(3)	8b

[a, b] the crystal has two crystallographically independent molecules; L = the corresponding NSiN ligand

Computational study of the Ir-Si bond in Ir-NSiN complexes.

To understand the bonding situation of the above complexes, a computational study using state-of-the-art methods, namely Atoms In Molecules (AIM),[25] Natural Bond Orbital (NBO)[26] and Energy Decomposition Analysis-Natural Orbital for Chemical Valence (EDA-NOCV)[27-28] methods, has been carried out.

We first explored the bonding situation of complexes **6** and **8** as representative systems having a short Ir–Si bond (~2.22 Å, Table 1). Figure 5 shows the Laplacian distribution of complex **6** in the O–Ir–Si plane. As expected, the AIM method confirms the occurrence of two five-membered iridacycles possessing one Ir–Si and two Ir–N bond critical points (BCPs) together with their associated bond paths (BPs) running between these atoms. The topology of both iridacycles is further confirmed by the presence of a ring critical point (RCP) located approximately in the center of each metallacycle. In addition, there exist BCPs between the C–H bonds of the pyridyl and coe ligands and the highly electronegative oxygen and fluorine atoms of the OTf ligand which indicates the occurrence of stabilizing noncovalent C-H···X interactions in this species. Despite that, these interactions are relatively weak in view of the computed rather low Wiberg bond indices (WBIs < 0.015) and NBO-second-order perturbation theory energies ($\Delta E^{(2)}$ = 1.8 kcal/mol). A similar topology is found for complex **8** (see Figure S1 in the ESI).

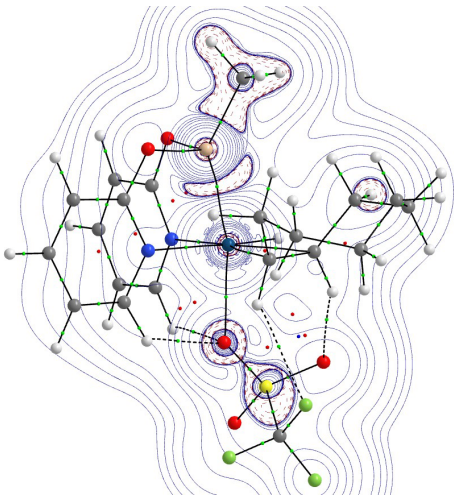

Figure 5. Contour line diagrams $\nabla^2\rho(r)$ for complex **6** in the O–Ir–Si plane. The solid lines connecting the atomic nuclei are the bond paths while the small green and red spheres indicate the corresponding bond critical points and ring critical points, respectively.

According to the data gathered in Table 2, it becomes evident that the nature of the Ir–Si bond is rather different from that of the Ir–N bonds. In particular, there is a noticeable difference in the computed values of the Laplacian of the electron density ($\nabla^2\rho(r_c)$) at the BCPs. Whereas positive values were computed for the Ir-N bonds, negative values were found for the Ir-Si. Typically, positive values of $\nabla^2\rho(r_c)$ indicate that the charge is locally depleted and, then, corresponds to "closed shell" (donor–acceptor or van der Waals) interactions while negative values reveal local charge accumulations, characteristic of covalent (electron-sharing) interactions. Therefore, our calculations indicate that whereas the Ir–N bond can be viewed, as expected, as dative N→Ir (donor-acceptor) bonds, the Ir–Si bond should be described as σ-covalent (electron-sharing) bond. Similar values were found by some of us in related Ir(III)-silylene complexes.[21c] Not surprisingly, the computed delocalization index, δ, which has been suggested as a measure of the relative bond strength,[29] indicates that the Ir–Si bond (δ = 0.93) is significantly stronger than both dative (i.e. donor-acceptor) Ir–N bonds (δ = 0.62 and 0.50), which agrees with the expected higher bond strength of a covalent bond than that of a dative bond. A similar result is found by applying the NBO method as the computed Wiberg bond index (WBI) for the Ir–Si (0.76) is markedly higher than the values computed for the Ir–N bonds (WBI = 0.37 and 0.19, respectively). These findings are also in agreement with the observed reactivity of complex **1** with excess of PMe_3 (Scheme 2)[10b] which indicates that the Ir–N bond is more labile than the Ir–Si bond.

Table 2. DFT calculated properties for the Ir–Si and Ir–N bonds in Ir-(*fac*-κ³-NSiN) complexes **6** and **8**. Results of the topological analysis of the electron density distribution: density, $\rho(r_c)$, Laplacian, $\nabla^2\rho(r_c)$, total energy density, $H(r_c)$ and delocalization index, d.

	6		**8**	
	Ir–Si	Ir–N	Ir–Si	Ir–N
$\rho(r_c)$	0.1115	0.0771 (0.0937)	0.1105	0.0762 (0.0932)
$\nabla^2\rho(r_c))$	−0.1470	+0.3545 (+0.4172)	−0.1470	+0.3488 (+0.4150)
$H(r_c)$	−0.0802	−0.0083 (−0.0149)	−0.0741	−0.0079 (−0.0147)
δ	0.93	0.50 (0.62)	0.95	0.49 (0.61)
WBI	0.76	0.19 (0.37)	0.74	0.19 (0.37)

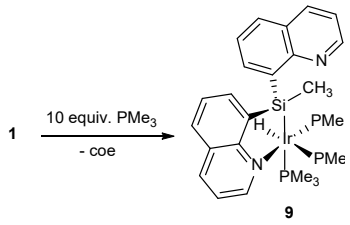

Scheme 2. Reactivity of complex **1** with excess of PMe_3.

To further clarify the nature of the Ir–Si bond in these species, we applied the EDA-NOCV method. To this end, this bond was analyzed in two different partitioning schemes using the $NSiN^{OPy}$ ligand and [Ir(H)(coe)OTf] as fragments, namely (i) charged $[NSiN^{OPy}]^-$ and $[Ir(H)(coe)OTf]^+$, where the interaction consists of two dative N→Ir bonds and one dative Si→Ir bond, and (ii) neutral $[NSiN^{OPy}]^\bullet$ and $[Ir(H)(coe)OTf]^\bullet$ fragments, which describes the bonding as two dative N→Ir bonds and one covalent (i.e. electron-sharing) Ir–Si bond. The calculation that gives the smallest orbital term ΔE_{orb} (i.e. involving the smallest change in the electronic structure of the fragments by the bond formation), is typically considered as the more reasonable description of the bond.[30,31] Therefore, according to the numerical results gathered in Table 2 for complex **6**, the bonding situation of this species is better described as possessing two dative N→Ir bonds and a covalent Ir–Si bond, which is fully consistent with the nature of the Ir–Si and Ir–N bonds initially suggested by the AIM and NBO methods (see above).

Data in Table 3 indicates that, despite using neutral fragments, the electrostatic attraction between the fragments (measured by the ΔE_{elstat} term) is stronger than the orbital interactions (ΔE_{orb}), which confirms that the ionic contribution to the bonding is remarkable (59% to the total attractive interactions). This is consistent with the Interacting Quantum Atoms (IQA)[32] approach which indicates that the ionic contribution to the Ir–Si bond is remarkable (71%).[33] This is not surprising according to the computed highly positive NBO charge at the silicon atom (q = +1.68), which indicates that the Si–IrO bond is highly polarized (charge of the IrO group −0.81). This can easily visualized by the molecular electrostatic potential computed for **6**, which clearly identifies the positivily charged silion atom (Figure 6). Despite that, three main orbital interactions are identified in complex **6** using the NOCV extension of the EDA method,[34] namely ρ_1, which involves the covalent σ-Ir–Si bond, ρ_2 and ρ_3, which involve both dative N→Ir bonds, and ρ_4, which consists of the π-backdonation from a double-occupied d(Ir) atomic orbital to a vacant p_π(Si) atomic orbital (see Figure 7). As clearly seen in Figure 6, the strength of the σ-Ir-Si bond ($\Delta E_{(\rho 1)}$ = −95.2 kcal/mol) is much higher than both dative N→Ir bonds ($\Delta E_{(\rho 2+\rho 3)}$ = −57.5 kcal/mol), which is consistent with the AIM-delocalization and NBO-Wiberg bond indices commented above. The Ir→Si π-backdonation is, not surprisingly, comparatively much weaker but not negligible ($\Delta E(\rho_4)$ = −13.0 kcal/mol), which is in line with previous studies.[13,14]

Table 3. EDA results (in kcal/mol) for complex **6** computed at the ZORA-BP86-D3/TZ2P//BP86-D3/def2-SVP level.

	3 dative bonds (2 N→Ir + Si→Ir)	**2 N→Ir dative bonds + Ir–Si covalent bond**
Fragments	$[Ir(H)OTf]^+ + [NSiN]^-$	$[Ir(H)OTf]^\bullet + [NSiN]^\bullet$
ΔE_{int}	−341.1	−185.9
ΔE_{Pauli}	406.8	376.6
ΔE_{elstat}	−432.8	−331.7
ΔE_{orb}	−294.7	−210.5
ΔE_{disp}	−20.4	−20.4

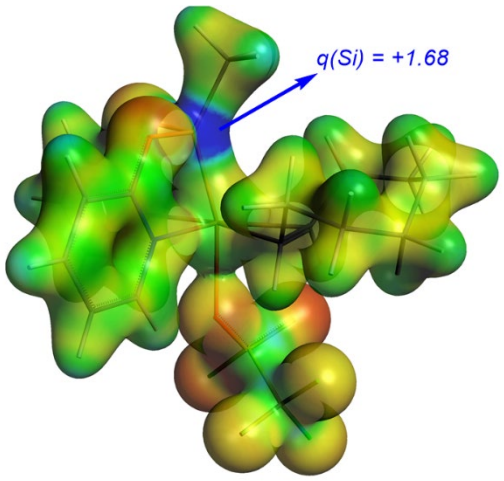

Figure 6. Plot of the molecular electrostatic potential computed for **6**.

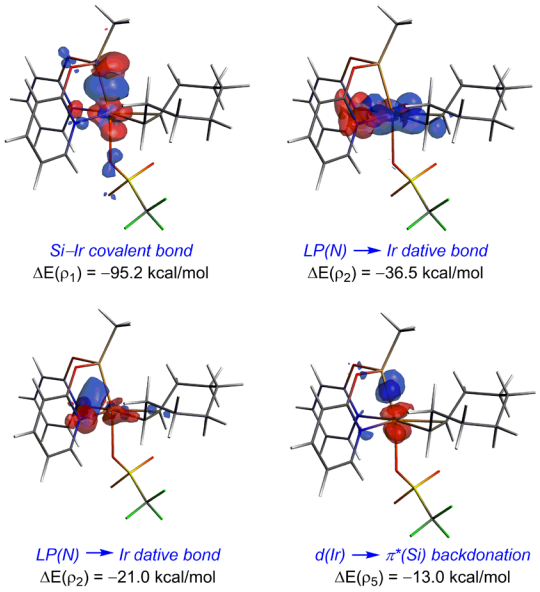

Figure 7. NOCV-deformation densities and associated stabilization energies computed for complex **6**. The charge flow takes place in the direction red → blue.

Once the general bonding situation of the Ir-NSiN complexes has been described, we then applied the EDA-NOCV method to quantitatively investigate the influence of the NSiN ligand, transition metal and surrounding ligands on the bonding. To this end, we selected the complexes **1** and **11**, and **6** and **10** having the $NSiN^{Q}$ or $NSiN^{OPy}$ ligands, respectively, in *fac*-κ^3-coordination mode and chloride or triflate as axial (to Si) ligands (see Table 3 and Figure 7). We also analyzed complex **8** having the axial CF_3CO_2 ligand and **7M**, a model compound of **7** where the cyclohexyl groups of the phosphane ligand were replaced by methyl groups, to study the influence of a phosphane σ-donor instead of the cyclooctene ligand. For completeness, the experimentally known rhodium(III)-complex [RhH(CF_3SO_2)(*fac*-κ^3-$NSiN^{OPy}$)(coe)] (**12**)[9] (Figure 8) has also been considered in our analysis to explore the influence of having a different group 9 transition metal.

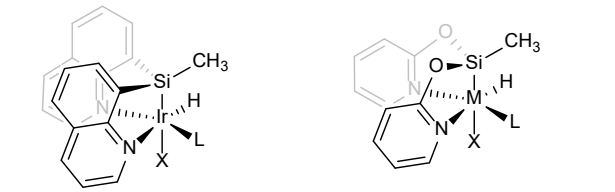

M = Ir; X = Cl; L = η^2-coe; (**1**)
M = Ir; X = OTf; L = η^2-coe; (**11**)
M = Ir; X = OTf; L = η^2-coe; (**6**)
M = Ir; X = Cl; L = PMe_3; (**7M**)
M = Ir; X = CF_3CO_2; L = η^2-coe; (**8**)
M = Ir; X = Cl; L = η^2-coe; (**10**)
M = Rh; X = OTf; L = η^2-coe; (**12**)

Figure 8. M-(*fac*-κ^3-NSiN) (M = Ir or Rh) complexes studied computationally.

From the data in Table 4, it becomes evident that the interaction (ΔE_{int}) between the [NSiN]• and [Ir(H)(coe)(X)]• (X = Cl or TfO) is stronger when a triflate (complexes **6** and **11**) instead of a chloride (complexes **1** and **10**) ligand is placed *trans* to the Si-moiety. This is supported by the corresponding Ir–Si WBIs, which are systematically higher in the OTf-complexes. The stronger interaction can be mainly ascribed to the higher electron-withdrawing nature of the OTf group, which further polarizes the Ir–Si bond resulting in a much stronger electrostatic attraction ($\Delta\Delta E_{elstat}$ = 8.7 and 6.9 kcal/mol, when comparing **6** vs **10** and **1** vs **11**, respectively). Not surprisingly, this enhanced Ir–Si bond polarization is also reflected in a higher positive charge at the silicon center in the OTf complexes (Δq = +0.1e when comparing **6** vs **10** and **1** vs **11**). Although the effect of the Cl/OTf replacement on the total orbital interactions (ΔE_{orb}) is not significant, the π-backdonation is slightly stronger in those complexes having the OTf ligand. Therefore, our EDA-NOCV calculations suggest that, regardless of the nature of the NSiN ligand, the axial OTf ligand mainly enhances the stabilizing electrostatic interactions, resulting in a clear shortening of the Ir–Si bond. Not surprisingly, a similar effect is found in complex **8**, having the highly electron-withdrawing CF_3CO_2 ligand in the apical position. According to the computed EDA and NBO data, the CF_3CO_2 is a slightly less electron-withdrawing group as compared to the CF_3SO_3 group (i.e. CF_3CO_2 leads to a lower interaction and electrostatic attraction, the charge on Si is also lower as well as the Ir–Si WBI as compared to the OTf group), which nicely agrees with their corresponding σ_p-Hammett constants (0.46 vs 0.53, for CF_3CO_2 and CF_3SO_3, respectively).[35]

The influence of the nature of the NSiN ligand on the Ir–Si interaction resembles that of the OTf ligand but is significantly more pronounced. Indeed, the electrostatic attractions become even much stronger in those complexes having the $NSiN^{OPy}$ instead of the $NSiN^{Q}$ ligand ($\Delta\Delta E_{elstat}$ = 14.3 and 16.1 kcal/mol, when comparing **1** vs **10** and **6** vs **11**, respectively). This effect is also reflected in the much higher polarization of the Ir–Si bond in the $NSiN^{OPy}$-complexes, whose silicon atoms exhibit the highest positive charges of the entire series (Δq = +0.3, when comparing **1** vs **10** and **6** vs **11**, respectively). As a result, complex **6** having the $NSiN^{OPy}$ and the axial OTf ligands exhibits the shortest Ir–Si bond length of the studied complexes, and, as expected, also the highest Ir–Si WBI (0.76).

According to the computed lower interaction, the replacement of the cyclooctene ligand by the strong σ-donor PMe_3 ligand (complexes **7M** vs **10**) makes the Ir–Si interaction slightly weaker. This is not because the key electrostatic interactions are lower (indeed, ΔE_{elstat} is 3 kcal/mol is higher in complex **7M** and the silicon charge is nearly identical) but to a significant weakening of the total orbital interactions, and particularly, the strong σ-Ir–Si covalent bond ($\Delta E_{(\rho1)}$ = -4.3 kcal/mol) and dative N→Si bonds ($\Delta E_{(\rho2+\rho3)}$ = -8.6 kcal/mol).

Table 4. EDA results (in kcal/mol) computed at the ZORA-BP86-D3/TZ2P//BP86-D3/def2-SVP level.

	1	6	7M	8	10	11	12
ΔE_{int}	-173.5	-185.9	-170.6	-182.9	-176.8	-185.4	-160.0
ΔE_{Pauli}	356.5	376.6	371.8	376.4	374.3	358.2	308.2
ΔE_{elstat}	-308.7	-331.7	-326.0	-328.8	-323.0	-315.6	-265.6
ΔE_{orb}[a]	-201.4	-210.5	-199.4	-210.8	-209.7	-205.5	-182.3
$\Delta E_{(\rho 1)}$	-92.6	-95.2	-93.6	-97.6	-97.9	-91.8	-91.3
$\Delta E_{(\rho 2+\rho 3)}$	-53.1	-57.5	-45.3	-53.8	-53.9	-57.7	-42.8
$\Delta E_{(\rho 4)}$	-9.5	-13.0	-12.9	-12.7	-12.4	-9.7	-10.0
ΔE_{disp}	-19.9	-20.4	-17.0	-19.7	-18.4	-22.5	-20.2
r(Si–M)[b]	2.307	2.252	2.258	2.260	2.268	2.290	2.226
	(2.275)	(2.219)	(2.224)	(2.223)			(2.139)
NBO q(Si)	+1.31	+1.68	+1.60	+1.64	+1.61	+1.38	
NBO q(Ir–X)[c]	-0.42	-0.81	-0.44	-0.55	-0.45	-0.76	
WBI (Si–M))	0.66	0.76	0.70	0.74	0.67	0.73	0.67

[a] Only the main orbital contributions ($\Delta E(\rho)$) to the total orbital interactions (ΔEorb) are given. [b] Bond lengths are given in angstroms. Values within parentheses indicate the experimental (X-ray) values. [c] X refers to the atom attached to iridium placed trans to silicon (X = Cl, O).

Finally, we analyzed the effect of the transition metal by comparing the Ir(III)-complex **6** with its Rh(IIII)-counterpart **12**, both having the NSiN^{OPy} and the axial OTf ligands. From the data in Table 3, it becomes clear that the interaction between the neutral [NSiN^{OPy}]$^{\bullet}$ and [Rh(H)(coe)OTf]$^{\bullet}$ fragments is comparatively weaker than that involving [Ir(H)(coe)OTf]$^{\bullet}$. According to the EDA-NOCV data, the replacement of Ir(III) by Rh(III) leads to a rather significant weakening of the key electrostatic interactions ($\Delta\Delta E_{elstat}$ = 66.2 kcal/mol). The orbital interactions are also less stabilizing albeit to a much lesser extent ($\Delta\Delta E_{orb}$ = 28.2 kcal/mol). This significant decrease of the electrostatic (and orbital) interactions makes the Rh–Si bond comparatively weaker than the Ir–Si bond, a result which is also supported by the corresponding WBIs (WBI = 0.76 and 0.67, for **6** and **12**, respectively).

Results described above therefore suggest that the electrostatic interactions play a key role in the Ir–Si interaction and, consequently, have a direct impact on the corresponding bond length. This is confirmed by plotting the computed ΔE_{elstat} values versus the computed Ir–Si bond lengths, which indicates that both parameters are nicely correlated (correlation coefficient of 0.97, Figure 9). The key role of the electrostatic interactions is further supported by the trend in the polarization of the Ir–Si bond, measured by the computed NBO charge at the silicon atom, which also exhibits a nice linear relationship with the Ir–Si bond lengths (R^2 = 0.96, see Figure S2 in the ESI). Moreover, although a similar linear relationship was also found when plotting the π-backdonation ($\Delta E_{(\rho 4)}$) vs the Ir–Si distances (R^2 = 0.94, see Figure S3), the influence of this weak orbital interaction on the Ir–Si bond can be considered as almost negligible when compared to the much stronger electrostatic interactions.

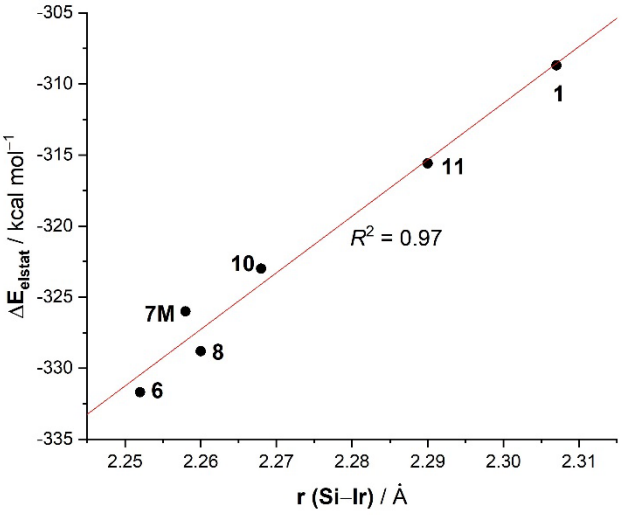

Figure 9. Plot of the computed electrostatic interactions (ΔE_{elstat}) vs the Si–Ir bond length.

To broaden the scope of the present study and rule out the influence of the pincer ligand on the bonding of the considered Ir-(fac-κ^3-NSiN) complexes, and in particular, on the rather short Ir–Si distances, we also considered the complexes **13** and **14**, as model complexes of the experimentally described [IrH_2{Si(OTf)Ph_2}(TFB) ($PiPr_3$)][16] and [$IrH_2(SiEt_3)$(cod)($AsPh_3$)],[36] where the bulky iPr and phenyl ligands where replaced by methyl groups. Both non-pincer compounds exhibit much longer Si–Ir distances of 2.376 Å and 2.444 Å. Despite that, the corresponding EDA data (Table 5) confirms that, even in this non-strained species, the electrostatic term dominates over the orbital term, which fully support the key role of the electrostatic interactions in the bonding situation of these Ir-Si complexes. Not surprisingly, from a quantitative point of point, the ΔE_{elstat} term in these compounds (as well as the total interaction energy) is much lower than in the constrained Ir-(fac-κ^3-NSiN) species, which mainly derives from the much longer Ir-Si distances in **13** and **14**.

Table 4. EDA results (in kcal/mol) for complexes **13** and **14** computed at the ZORA-BP86-D3/TZ2P//BP86-D3/def2-SVP level.

	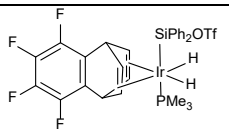	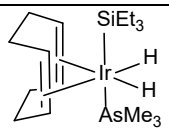
	13	**14**
ΔE_{int}	–104.1	–88.0
ΔE_{Pauli}	234.5	206.7
ΔE_{elstat}	–184.2	–169.8
ΔE_{orb}	–129.7	–107.9
ΔE_{disp}	–24.7	–17.1
r(Si–Ir) / Å	2.376	2.444

Experimental Section

Statistical analysis of the Ir–Si bond length

The statistical analysis of the Ir–Si bond lengths has been carried out with the Cambridge Structural Database (CSD).[23] The search of the Ir-Si fragment has been performed using ConQuest 2020.3.0 program[24] and the database version 5.42 (November 2020). Polymeric, error-containing, powder structures and structures with R factor higher than 0.1 were removed from our dataset. The 235 results (334 Ir-Si fragments) are listed in the ESI.

Computational details

Geometry optimization of all complexes was performed without symmetry constraints using the Gaussian09[37] suite of programs at the BP86[38]/def2-SVP[39] level of theory using the D3 dispersion correction suggested by Grimme et al.[40] This level is denoted BP86-D3/def2-SVP. All species were also characterized by frequency calculations and have positive definite Hessian matrices thus confirming that the computed structures are minima on the potential energy surface. Wiberg Bond Indices (WBIs) have been computed using the natural bond orbital (NBO) method.[25] All AIM[26] results described in this work correspond to calculations performed at the BP86-D3/6-31+G(d)/WTBS (for Ir and Rh) level on the optimized geometry obtained at the BP86-D3/def2-SVP level. The WTBS (well-tempered basis sets)[41] have been recommended for AIM calculations involving transition metals.[42] The topology of the electron density was conducted using the AIMAll program package.[43]

The interaction between the selected fragments has been investigated with the EDA-NOCV method,[27-28] which combines the energy decomposition analysis (EDA)[27] with the natural orbitals for chemical valence (NOCV)[28] methods. Within this approach, the interaction energy can be decomposed into the following physically meaningful terms:

$$\Delta E_{int} = \Delta E_{elstat} + \Delta E_{Pauli} + \Delta E_{orb} + \Delta E_{disp}$$

The term ΔE_{elstat} corresponds to the classical electrostatic interaction between the unperturbed charge distributions of the deformed reactants and is usually attractive. The Pauli repulsion ΔE_{Pauli} comprises the destabilizing interactions between occupied orbitals and is responsible for any steric repulsion. The orbital interaction ΔE_{orb} accounts for charge transfer (interaction between occupied orbitals on one moiety with unoccupied orbitals on the other, including HOMO–LUMO interactions) and polarization (empty-occupied orbital mixing on one fragment due to the presence of another fragment). Finally, the ΔE_{disp} term takes into account the interactions which are due to dispersion forces.

The EDA-NOCV method makes it possible to further partition the total orbital interactions into pairwise contributions of the orbital interactions. Details of the method can be found in the literature.

The EDA-NOCV calculations were carried out using the BP86-D3/def2-SVP optimized geometry with the program package ADF 2019.01[44] using the same functional (BP86-D3) in conjunction with a triple-ζ-quality basis set using uncontracted Slater-type orbitals (STOs) augmented by two sets of polarization function with a frozen-core approximation for the core electrons.[45] An auxiliary set of s, p, d, f, and g STOs were used to fit the molecular densities and to represent the Coulomb and exchange potentials accurately in each SCF cycle.[46] Scalar relativistic effects were incorporated by applying the zeroth-order regular approximation (ZORA).[47] This level of theory is denoted ZORA-BP86-D3/TZ2P//BP86-D3/def2-SVP and has been selected because of its good performance to describe the bond situation of transition metal complexes.[48]

Conclusions

A statistical analysis of the Ir–Si bond length of the structures deposited in the Cambridge Structural Database (CSD) using ConQuest program shows a median value for the Ir–Si bond distance of 2.34 Å. This analysis confirms that the Ir–Si bond lengths in Ir-(*fac*-κ^3-NSiN) species are in the lowest limit of the reported bond distances. In particular, complex **6** having the *fac*-κ^3-NSiN^{OPy} ligand and a triflate ligand (axial to the silicon atom) exhibits the shortest Ir–Si bond length (2.22 Å). This remarkable bond shortening was initially attributed either to the occurrence of π-backbonding from *d*-metal orbitals to empty silicon orbitals, or alternatively, to the ionic contribution to the bonding.[13-15]

Our calculations suggest that the Ir–Si bond in these complexes can be described as an electron-sharing (i.e. covalent) bond. Despite that, this bond is highly polarized which makes the contribution of the electrostatic attractions to the bonding rather significant. This contribution has a direct impact on the

corresponding bond length. Indeed, the computed ΔE_{elstat} values, which are a measure of the ionic contribution to the bonding, are nicely correlated with the computed Ir–Si bond lengths ($R^2 = 0.97$). Our calculations also confirm the occurrence of the previously proposed π-backdonation ($\Delta E_{(\rho 4)}$).[13] However, the contribution of this orbital interaction to the Ir–Si interaction is rather weak (around -9.5 and -13.0 kcal/mol) and can be therefore considered as negligible when compared to the much stronger electrostatic interactions (ranging from −308.7 to −331.7 kcal/mol). Both contributors, i.e. the electrostatic attractions and the orbital π-backdonation, are higher in Ir-(*fac*-κ^3-NSiN^{OPy}) species than in Ir-(*fac*-κ^3-NSiN^{Q}) derivatives, the former typically exhibiting shorter Ir–Si bonds.

In short, our quantitative description of the bonding situation of Ir-(*fac*-κ^3-NSiN) complexes allows us to conclude that the remarkable Ir–Si bond shortening in these species can be mainly attributed to the electrostatic (i.e. ionic) contribution to the bonding.

Conflicts of interest

There are no conflicts to declare.

Acknowledgements

The financial support from MINECO/FEDER (projects PGC2018-099383-B-I00, PID2019-106184GB-I00, and RED2018-102387-T) and DGA/FSE project E42_20R is gratefully acknowledged. We thank Prof. A. Martín Pendás for his assistance with the IQA method.

Notes and references

1 (a) F. J. Fernández-Alvarez, R. Lalrempuia and L. A. Oro, *Coord. Chem. Rev.* 2017, **350**, 49-60; (b) M. Simon and F. Breher, *Dalton Trans.* 2017, **46**, 7976-7997.

2 F. L. Joslin and S. R. Stobart, *J. Chem. Soc., Chem. Commun.* 1989, 504-505.

3 (a) M. C. McInnis, D. F. MacLean, R. J. Lundgren, R. McDonald and L. Turculet, *Organometallics* 2007, *26*, 6522-6525; (b) D. F. MacLean, R. McDonald, M. J. Ferguson, A. J. Caddell and L. Turculet, *Chem. Commun.* 2008, 5146-5148; (c) E. Morgan, D. F. MacLean, R. McDonald and L. Turculet, *J. Am. Chem. Soc.* 2009, **131**, 14234-14236.

4 (a) E. Sola, A. García-Camprubí, J. L. Andrés, M. Martín and P. Plou, *J. Am. Chem. Soc.* 2010, **132**, 9111-9121; (b) A. García-Camprubí, M. Martín and E. Sola, *Inorg. Chem.* 2010, **49**, 10649-10657; (c) E. Suárez, P. Plou, D. G. Gusev, M. Martín and E. Sola, *Inorg. Chem.* 2017, **56**, 7190-7199; (d) R. Webber, M. I. Qadir, E. Sola, M. Martín, E. Suárez and J. Dupont, *Catal. Commun.* 2020, **146,** 106125.

5 (a) M. T. Whited, A. M. Deetz, J. W. Boerma, D. E. DeRosha and D. E. Janzen, *Organometallics* 2014, **33**, 5070-5073; (b) M. T. Whited, A. M. Deetz, T. M. Donnell and D. E. Janzen, *Dalton Trans.* 2016, **45**, 9758-9761; (c) M. T. Whited, J. Zhang, T. M. Donnell, V. H. Eng, P. O. Peterson, M. J. Trenerry, D. E. Janzen and B. L. H. Taylor, *Organometallics* 2019, **38**, 4420-4432; (d) M. T. Whited, M. J. Trenerry, K. E. DeMeulenaere and B. L. H. Taylor, *Organometallics* 2019, **38**, 1493-1501.

6 (a) H. Kameo, S. Ishii and H. Nakazawa, *Dalton Trans.* 2013, **42**, 4663-4669; (b) H. Kameo, T. Kawamoto, S. Sakaki, D. Bourissou and H. Nakazawa, *Chem. Eur. J.* 2016, **22**, 2370-2375.

7 (a) Y. H. Li, Y. Zhang and X.-H. Ding, *Inorg. Chem. Commun.* 2011, **14**, 1306-1310; (b) H. Fang, Y.-K. Choe, Y. Li and S. Shimada, *Chem. Asian J.* 2011, **6**, 2512-2521.

8 (a) R. Lalrempuia, M. Iglesias, V. Polo, P. J. Sanz Miguel, F. J. Fernández-Alvarez, J. J. Pérez-Torrente and L. A. Oro, *Angew. Chem. Int. Ed.* 2012, **51**, 12824–12827; (b) A. Julián, E. A. Jaseer, K. Garcés, F. J. Fernández-Alvarez, P. García-Orduña, F. J. Lahoz and L. A. Oro, *Catal. Sci. Technol.* 2016, **6**, 4410–4417; (c) A. Julián, J. Guzmán, E. A. Jaseer, F. J. Fernández-Alvarez, R. Royo, V. Polo, P. García-Orduña, F. J. Lahoz and L. A. Oro, *Chem. Eur. J.* 2017, **23**, 11898–11907; (d) A. Julián, K. Garcés, R. Lalrempuia, E. A. Jaseer, F. J. Fernández-Alvarez, P. García-Orduña, F. J. Lahoz and L. A. Oro, *ChemCatChem* 2018, **10**, 1027–1034.

9 K. Garcés, R. Lalrempuia, V. Polo, F. J. Fernández-Alvarez, Pilar García-Orduña, F. J. Lahoz, J. J. Pérez-Torrente and L. A. Oro, *Chem. Eur. J.* 2016, **22**, 14717–14729.

10 (a) M. Stradiotto, K. L. Fujdala and T. D. Tilley, *ChemCommun* 2001, 1200–1201; (b) P. Sangtrirutnugul and T. D. Tilley, *Organometallics* 2007, **26**, 5557–5568; (c) P. Sangtrirutnugul, M. Stradiotto and T. D. Tilley, *Organometallics* 2006, **25**, 1607–1617.

11 (a) S. Azpeitia, B. Fernández, M. A. Garralda and M. A. Huertos, *Eur. J. Inorg. Chem.* 2015, 5451–5456; (b) S. Azpeitia, A. Rodríguez-Diéguez, M. A. Garralda and M. A. Huertos, *ChemCatChem* 2018, **10**, 2210–2213; (c) N. Almenara, J. I. Miranda, A. Rodríguez-Diéguez, M. A. Garralda and M. A. Huertos, *Dalton Trans.* 2019, **48**, 17179–17183.

12 (a) J. Zhu, Z. Lin and T. B. Marder, *Inorg. Chem.* 2005, **44**, 9384-9390; (b) B. J. Coe and S. J. Glenwright, *Coord. Chem. Rev.* 2000, **203**, 5-80.

13 (a) T. D. Tilley, *Transition-metal silyl derivatives*, in *The Chemistry of organic silicon compounds*. *Part 2*, S. Patai and Z. Rappoport, Eds, John Wiley & Sons, Chichester, 1989; (b) D. L. Lichtenberger and A. Rai-Chaudhuri, *J. Am. Chem. Soc.* 1991, **113**, 2923-2930.

14 M. T. Whited and B. L. H. Taylor, *Comments Inorg. Chem.* 2020, **40**, 217–276 and references therein.

15 D. H. Binh, M. Milovanović, J. Puertes-Mico, M. Hamdaoui, S. D. Zarić and J.-P. Djukic, *Chem. Eur. J.* 2017, **23**, 17058–17069.

16 W. Chen, A. J. Edwards, M. A. Esteruelas, F. J. Lahoz, M. Oliván and L. A. Oro, *Organometallics* **1996**, *15*, 2185–2188.

17 (a) M. E. Fasulo, P. B. Glaser and T. D. Tilley, *Organometallics* 2011, **30**, 5524–5531; (b) J. D. Feldman, J. C. Peters and T. D. Tilley, *Organometallics* 2002, **21**, 4065–4075; (c) S. R. Klei, T. D. Tilley and R. G. Bergman, *Organometallics* 2002, **21**, 3376–3387; (d) J. C. Peters, J. D. Feldman and T. D. Tilley, *J. Am. Chem. Soc.* 1999, **121**, 9871–9872.

18 (a) D. H. Binh, M. Hamdaoui, D. Fischer-Krauser, L. Karmazin, C. Bailly and J.-P. Djukic, *Chem. Eur. J.* 2018, **24**, 17577–17589; (b) J. A. Cabeza, P. García-Álvarez and L. González-Álvarez, *Chem. Commun.* 2017, **53**, 10275-10278.

19 H. Hashimoto, T. Suzuki and H. Tobita, *Dalton Trans.* 2010, **39**, 9386–9400.

20 (a) E. Calimano and T. D. Tilley, *J. Am. Chem. Soc.* 2009, **131**, 11161–11173; (b) E. Calimano and T. D. Tilley, *Dalton Trans.* 2010, **39**, 9250–9263.

21 (a) J. Guzmán, P. García-Orduña, V. Polo, F. J. Lahoz, L. A. Oro and F. J. Fernández-Alvarez, *Catal. Sci. Technol.* 2019, **9**, 2858–2867; (b) J. Guzmán, P. García-Orduña, F. J: Lahoz and F. J. Fernández-Alvarez, *RSC Adv.* 2020*,* **10**, 9582–9586; (c) J. Guzmán, A. M. Bernal, P. García-Orduña, F. J. Lahoz, V. Polo and F. J. Fernández-Alvarez, *Dalton Trans.* 2020, **49**, 17665–17673.

22 J. Guzmán, A. M. Bernal, P. García-Orduña, F. J. Lahoz, L. A. Oro and F. J. Fernández-Alvarez, *Dalton Trans.* 2019, **48**, 4255–4262.

23 C.R. Groom, I. J. Bruno, M.P. Lightfoot and S.C. Ward, *Acta Cryst*. 2016, **B72**, 171-179.

24 I. J. Bruno, J. C. Cole, P. R. Edgington, M. Kessler, C. F. Macrae, P. McCabe, J. Pearson and R. Taylor, *Acta Cryst*. 2002, **B58**, 389-397.

25 (a) R. F. W. Bader, *Acc. Chem. Res*. 1985, **18**, 9–15; (b) R. F. W. Bader, *Chem. Rev*. 1991, **91**, 893–928; (c) R. F. W. Bader, Atoms in Molecules, A Quantum Theory; Oxford University Press: Oxford, U.K., 1990.Google Scholar

26 (a) J. P. Foster and F. Weinhold, *J. Am. Chem. Soc*. 1980, **102**, 7211–7218; (b) A. E. Reed and F. Weinhold, *J. Chem. Phys*. 1985, **83**, 1736–1740; (c) A. E. Reed, R. B. Weinstock and F. Weinhold, *J. Chem. Phys*. 1985, **83**, 735–746; (d) A. E. Reed, L. A. Curtiss and F. Weinhold, *Chem. Rev*. 1988, **88**, 899–926.

27 (a) F. M. Bickelhaupt and E. J. Baerends, in Reviews in Computational Chemistry (Eds.: K. B. Lipkowitz, D. B. Boyd), Wiley, Hoboken, 2000, pp. 1–86; (b) L. Zhao, M. von Hopffgarten, D. M. Andrada and G. Frenking, *WIREs Comput. Mol. Sci*. 2018, **8**, e1345.

28 M. P. Mitoraj, A. Michalak and T. Ziegler, *J. Chem. Theory Comput*. 2009, **5**, 962–975.

29 C. Outeiral, M. A. Vincent, A. Martín Pendás and P. L. A. Popelier, *Chem. Sci*. 2018, **9**, 5517–5529.

30 See, for instance: (a) J. C. Babón, M. A. Esteruelas, I. Fernández, A. M. López and E. Oñate, *Organometallics* 2018, **37**, 2014–2017; (b) L. Zhao, M. Hermann, W. H. E. Schwarz and G. Frenking, *Nat. Rev. Chem.* 2019, **3**, 48–63; (c) I. Fernández, N. Holzmann and G. Frenking, *Chem. Eur. J*. 2020, **26**, 14194–14210; (d) S. Pan, S. M. N. V. T. Gorantla, D. Parasar, H. V. R. Dias and G. Frenking, *Chem. Eur. J*. **2021**, doi: 10.1002/chem.202004041 and references therein.

31 Despite that, criticisms about the limitations of the EDA method have been recently highlighted. See, for instance: (a) P. Salvador, E. Vos, I. Corral and D, M. Andrada, *Angew. Chem. Int. Ed*. 2020, **60**, 1498-1502; (b) D. M. Andrada and C. Foroutan-Nejad, *Phys. Chem. Chem. Phys*. 2020, **22**, 22459-22464.

32 (a) A. Martín Pendás, M. A. Blanco and E. Francisco, *J. Chem. Phys*. 2004, **120**, 4581-4592; (b) A. Martín Pendas, E. Francisco and M. A. Blanco, *J. Comput. Chem*. 2004, **26**, 344-351; (c) M. A. Blanco, A. Martín Pendás and E. Francisco, *J. Chem. Theory Comput*. 2005, **1**, 1096-1109. For a recent review, see: J. M. Guevara-Vela, E. Francisco, T. Rocha-Rinza and A. Martín Pendás, *Molecules* 2020, **25**, 4028-4063.

33 The ionic contribution (IC) has been approximated to IC = (q_{Si} * q_{Ir}) / r_{Si-Ir} whereas the covalent contribution (CC) was computed as CC = -$\delta_{Ir\text{-}Si}$ / 2r_{Si-Ir}, where q, r, and δ stand for the computed charge, distance and delocalization index, respectively. See: A. Martín Pendás and E. Francisco, *Phys. Chem. Chem. Phys*. 2018, **20**, 16231-16237.

34 Besides these main orbital interactions, the NOCV method also identifies other interactions whose contribution to the total orbital interaction term ΔE_{orb} is much less significant ($\Delta E(\rho) < -10$ kcal/mol).

35 C. Hansch, A. Leo and R. W. Taft, *Chem. Rev*. 1991, **91**, 165-195.

36 M. J. Fernández, M. A. Esteruelas, L. A. Oro, M.-C. Apreda, C. Foces-Foces and F. H. Cano, *Organometallics*, **1987**, *6*, 1751–1756.

37 Gaussian 09, Revision D.01, M. J. Frisch, G. W. Trucks, H. B. Schlegel, G. E. Scuseria, M. A. Robb, J. R. Cheeseman, G. Scalmani, V. Barone, G. A. Petersson, H. Nakatsuji, X. Li, M. Caricato, A. Marenich, J. Bloino, B. G. Janesko, R. Gomperts, B. Mennucci, H. P. Hratchian, J. V. Ortiz, A. F. Izmaylov, J. L. Sonnenberg, D. Williams-Young, F. Ding, F. Lipparini, F. Egidi, J. Goings, B. Peng, A. Petrone, T. Henderson, D. Ranasinghe, V. G. Zakrzewski, J. Gao, N. Rega, G. Zheng, W. Liang, M. Hada, M. Ehara, K. Toyota, R. Fukuda, J. Hasegawa, M. Ishida, T. Nakajima, Y. Honda, O. Kitao, H. Nakai, T. Vreven, K. Throssell, J. A. Montgomery, Jr., J. E. Peralta, F. Ogliaro, M. Bearpark, J. J. Heyd, E. Brothers, K. N. Kudin, V. N. Staroverov, T. Keith, R. Kobayashi, J. Normand, K. Raghavachari, A. Rendell, J. C. Burant, S. S. Iyengar, J. Tomasi, M. Cossi, J. M. Millam, M. Klene, C. Adamo, R. Cammi, J. W. Ochterski, R. L. Martin, K. Morokuma, O. Farkas, J. B. Foresman, and D. J. Fox, Gaussian, Inc., Wallingford CT, 2016.BP86

38 (a) A. D. Becke, *Phys. Rev. A* 1988, **38**, 3098–3100; (b) J. P. Perdew,. *Phys. Rev. B* 1986, **33**, 8822–8824.

39 F. Weigend and R. Ahlrichs, *Phys. Chem. Chem. Phys*., 2005, **7**, 3297–3305.

40 S. Grimme, J. Antony, S. Ehrlich and H. Krieg, *J. Chem. Phys*. 2010, **132**, 154104.

41 (a) S. Huzinaga and B. Miguel, *Chem. Phys. Lett*. 1990, **175**, 289–291; (b) S. Huzinaga and M. Klobukowski, *Chem. Phys. Lett*. 1993, **212**, 260–264.

42 J. A. Cabeza, J. F. van der Maelen and S. García-Granda, *Organometallics* 2009, **28**, 3666–3672 and references therein.

43 T. A. Keith, AIMAll, 2010, http://tkgristmill.com.

44 (a) G. te Velde, F. M. Bickelhaupt, E. J. Baerends, C. Fonseca Guerra, S. J. A. van Gisbergen, J. G. Snijders and T. Ziegler, *J. Comput. Chem*. 2001, **22**, 931–967; (b) C. Fonseca Guerra, J. G. Snijders, G. te Velde and E. J. Baerends, *Theor. Chem. Acc*. 1998, **99**, 391–403; (c) ADF2018.104, SCM Theoretical Chemistry, Vrije Universiteit: Amsterdam (Netherlands). http://www.scm.com

45 J. G. Snijders, P. Vernooijs and E. J. Baerends, *At. Data. Nucl. Data Tables* 1981, **26**, 483–509.

46 A. Krijn and E. J. Baerends, *Fit Functions in the HFS-Method, Internal Report* (in Dutch), Vrije Universiteit Amsterdam, The Netherlands, 1984.

47 (a) E. van Lenthe, E. J. Baerends and J. G. Snijders, *J. Chem. Phys*. 1993, **99**, 4597–4610; (b) E. van Lenthe, E. J. Baerends and J. G. Snijders, *J. Chem. Phys*. 1994, **101**, 9783–9792; (c) E. van Lenthe, A. Ehlers and E. J. Baerends, *J. Chem. Phys*. 1999, **110**, 8943–8953.

48 Representative recent examples: (a) M. Baya, Ú. Belío, I. Fernández, S. Fuertes and A. Martín, *Angew. Chem. Int. Ed*. **2016**, *55*, 6978–6982; (b) J. C. Babón, M. A. Esteruelas, I. Fernández, A. M. López and E. Oñate, *Inorg. Chem*. **2019**, *58*, 8673–8684. See also reference 30.